JOM, Vol. 72, No. 1, 2020
https://doi.org/10.1007/s11837-019-03920-y

Estimating Powder-Polymer Material Properties Used in Design for Metal Fused Filament Fabrication (DfMF^3)

PARAMJOT SINGH,[1] QASIM SHAIKH,[1] VAMSI K. BALLA,[1,2] SUNDAR V. ATRE,[1] and KUNAL H. KATE [1,3]

1.—Materials Innovation Guild, University of Louisville, Louisville, KY 40208, USA 2.—CSIR-Central Glass and Ceramic Research Institute, Kolkata 700 032, India. 3.—e-mail: kunal.kate@louisville.edu

Metal fused filament fabrication (MF^3) combines fused filament fabrication and sintering processes to fabricate complex metal components. In MF^3, powder-polymer mixtures are printed to produce green parts that are subsequently debound and sintered. In the design for MF^3 (DfMF^3), it is important to understand how material properties of the filament affect processability, part quality, and ensuing properties. However, the materials property database of powder-polymer materials to perform DfMF^3 simulations is very limited, and experimental measurements can be expensive and time-consuming. This work investigates models that can predict the powder-polymer material properties that are required as input parameters for simulating the MF^3 using the Digimat-AM® process design platform for fused filament fabrication. Ti-6Al-4V alloy (56–60 vol.%) and a multicomponent polymer binder were used to predict properties such as density, specific heat, thermal conductivity, Young's modulus, and viscosity. The estimated material properties were used to conduct DfMF^3 simulations to understand material-processing-geometry interactions.

INTRODUCTION

Metal fused filament fabrication (MF^3) is a hybrid 3D printing process used to fabricate custom 3D metal components. MF^3 provides an alternative to other energy-intensive metal additive manufacturing (AM) processes such as laser-powder bed fusion, selective laser sintering, and direct energy deposition. MF^3 is a multi-step process that involves: (1) mixing and extrusion of a powder-polymer mixture into filaments, (2) 3D printing of a green part, (3) polymer removal from the 3D printed green part by debinding to get a brown part, and (4) densifying the brown part to achieve dense metal parts by sintering. Expected benefits of MF^3 include greatly expanding the property window of parts fabricated using the established fused filament fabrication (FFF) process, printing with mixed and multi-material systems, minimizing powder exposure at the printing stage, and expanding the range of materials available to current designers and users on the most widely used FFF platform.[1]

Figure 1a shows a typical process overview for MF^3 demonstrated by our group to fabricate Ti-6Al-4V alloy components. The powder-polymer mixtures used in MF^3 are adapted from metal injection molding (MIM) and are processed by modifying FFF process that typically fabricate polymeric parts.[1,2] Although materials design rules are known for processing powder-polymer mixtures using MIM, they cannot be directly applied to formulate new MF^3 materials owing to differences in physical phenomena involved in the two processes. Moreover, processing with polymers using FFF is well known, but very limited literature exists on the processing of polymer systems with high solid loadings (> 50 vol.%) typically used for MF^3.[1,3–7]

For example, in MIM, powder-polymer feedstocks are melt-processed at high shear rates in the range of 10^2–10^5 s^{-1}.[2] However, the FFF processing of a polymer is typically done at a shear rate in the range of 10–300 s^{-1}.[8] These differences pose significant processing challenges for powder-polymer mixtures that display shear-thinning behavior. Furthermore, other properties such as density,

(Published online November 12, 2019)

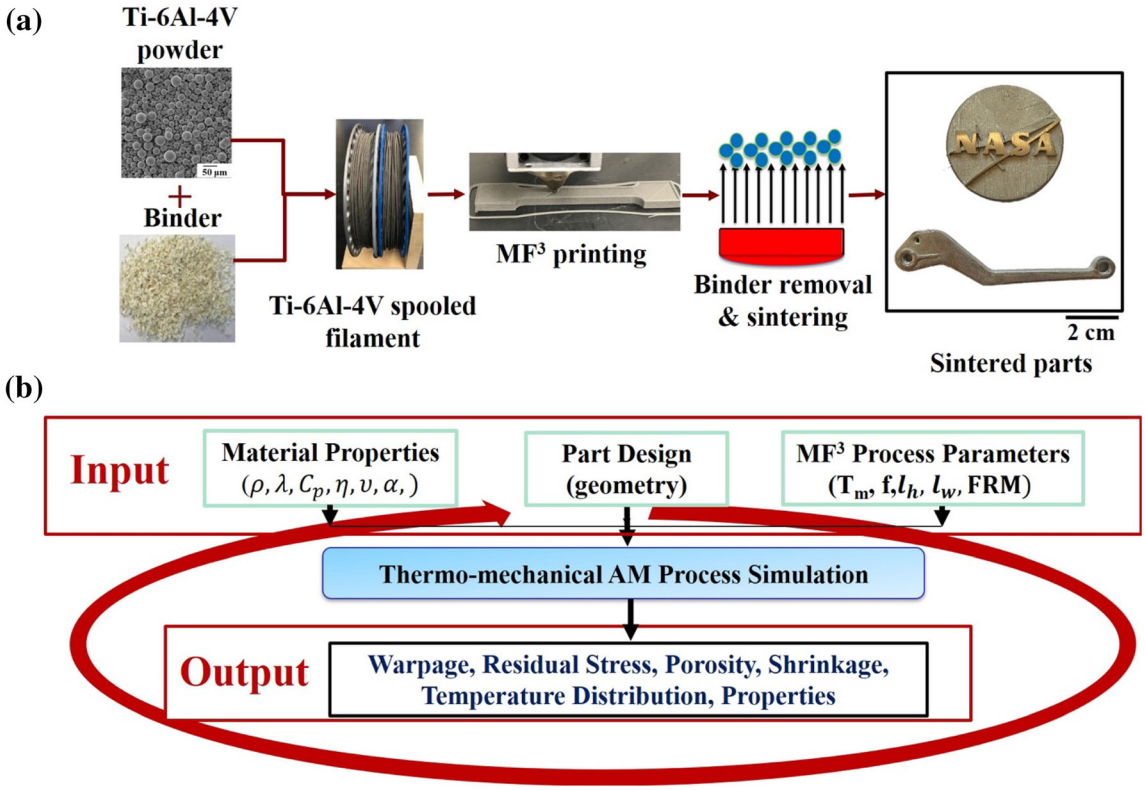

Fig. 1. (a) Process overview for MF^3 with examples of fabricated Ti-6Al-4V parts by our group, and (b) the present work for determining the input material parameters for conducting DfMF^3.

thermal, mechanical, and equation-of-state parameters (PVT) change with variation in powder-polymer concentrations. Any variations in powder-polymer composition can consequently affect filament properties, filament processing, 3D printing, debinding, and sintering. Accordingly, material compositional variations can affect the design of not only component geometrical attributes but also overhangs and support structures in the printed part. Figure 1b represents our present approach to capture material influences on processing and part attributes using a design-for-metal-fused-filament-fabrication (DfMF^3) platform.

Our current work on processing Ti-6Al-4V powder-polymer mixtures with MF^3 has examined several defects at different stages of MF^3 processing owing to compositional variations and their impact on processing and geometry (Fig. 2). Figure 2a and b were imaged using scanning electron microscopy (TESCAN Vega 3), and Fig. 2c and d were imaged using optical microscopy (Olympus BX-51). Figure 2a shows the presence of pores in the filament, leading to lower filament densities. These filaments were also found to buckle and crack under pressures exerted by the pinch roller during 3D printing owing to a lower strength. Figure 2b shows printing defects, such as gaps across layers within a cross section resulting in low green density in MF^3 parts, which can magnify post-sintering. Typical cracks occurring during debinding presumably because of the internal stresses in a part are presented in Fig. 2c. Finally, Fig. 2d shows the distribution of porosity within and between printing tracks and the gap between layers following sintering.

Understanding defect evolution during MF^3 processing will be crucial to achieve the desired material properties and part functionality. Specifically, simulation tools to correctly identify appropriate material compositions and process parameters for designing parts suitable for MF^3 can help reduce the trial and error involved in producing defect-free parts. As the density and thermal properties for metal-polymer systems are much higher than for an unfilled polymer, correct design protocols for parts with overhangs and support structures need to be identified with MF^3. The potential of the MF^3 process in fabricating metal parts has been shown in some of the published work for 17–4 PH stainless steel, copper, WC-10Co, W-Cr, and Cu-10Sn materials.[1,4,5,9–13] However, the use of design tools to perform material and process simulations in MF^3 has not yet been explored, thereby limiting the widespread use of the MF^3 process to manufacture parts with different materials for a variety of applications.[12]

Many FFF simulation platforms, such as Digimat-AM® (MSC Software), GENOA® (AlphaSTAR), and GENESIS® (Vanderplaats R&D), are commercially available and are currently being evaluated and adapted by us to conduct DfMF^3 simulations.

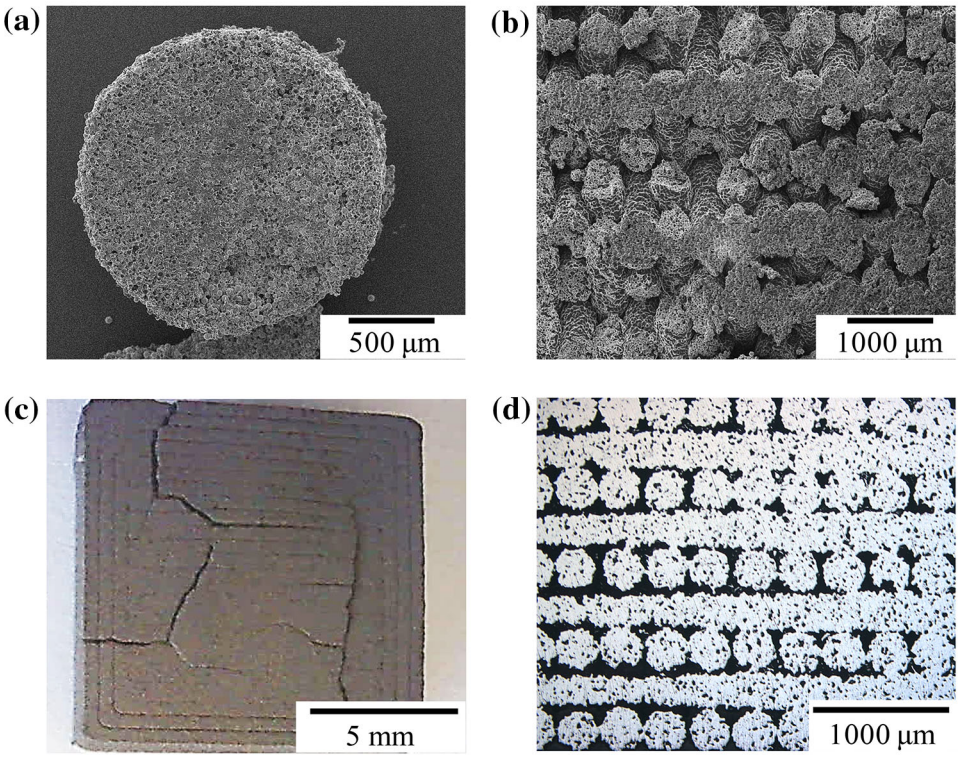

Fig. 2. Typical defects observed during the MF^3 process of the Ti-6Al-4V alloy system fabricated by our group showing (a) dark regions representing pores within a cut cross section of a powder-polymer filament, (b) gaps between layers within an MF^3 fabricated green part, (c) crack propagation observed after debinding, and (d) presence of pores present in the sintered MF^3 part (Color figure online).

Common to these simulation platforms is the need for a range of powder-polymer mixture material properties such as physical, thermal, mechanical, rheological, and equation-of-state parameters (PVT) as input parameters.[14–16] Compared with properties of $>$ 5000 different grades of plastics commonly used in injection molding simulation platforms, $<$ 10 polymeric material systems are available in the database of FFF simulation platforms and none for MF^3 materials. Any variations in powder concentrations or change in powder-polymer mixture material properties will require new experimental measurements to be performed, which can be time-consuming and expensive.

The current work addresses the important gap in the availability of powder-polymer properties for DfMF^3 by selecting material models that predict properties using metal properties available in the literature in conjunction with experimentally measured polymer matrix properties. To identify the influence of varying powder contents (solid loading, chemistry), properties were estimated for density, thermal conductivity, specific heat, modulus, coefficient of thermal expansion, viscosity as a function of shear rate and temperature, and specific volume as a function of pressure and temperature. The estimated material properties for the Ti-6Al-4V powder-polymer were used to understand simulation outputs such as warpages and dimensions using the DfMF^3 platform, Digimat-AM®. Furthermore, a comparison of warpage and dimensions between DfMF^3 simulations and 3D printing experiments was performed for a 59 vol.% solid loading Ti-6Al-4V powder-polymer material system. The output of the DfMF^3 study was compared with FFF simulations and experiments of an unfilled acrylonitrile butadiene styrene (ABS) polymer. It is expected that the overall approach will significantly reduce the trial and error in designing new materials used to fabricate complex MF^3 parts.

MODELS FOR POWDER-POLYMER MATERIAL PROPERTIES

Various models can predict material thermophysical properties for powder-polymer mixtures.[17–28] Our recent work compared various models used to predict the density, modulus, thermal conductivity, specific heat, viscosity, and specific volume and identified models that provided the best fit to experimental measurements of powder-polymer properties.[26,27,29] From the set of models screened for predicting material properties, models that provided the best fit (coefficient of regression R^2 fit of 0.87–0.99) with experimental measurements in prior work were selected. In the current work, a protocol was developed to use existing literature filler (powder) properties and experimentally measured binder properties in conjunction with the selected models to estimate the powder-polymer properties required to perform DfMF^3 simulations.

Material properties include density, thermal conductivity, specific heat, modulus, coefficient of thermal expansion, viscosity as a function of shear rate and temperature, and specific volume as a function of pressure and temperature. As a representative, yet high-impact material, Ti-6Al-4V alloy was used as the filler phase while experimentally measured properties of a wax-polymer binder were used as a matrix phase. Table I lists the thermomechanical properties of Ti-6Al-4V alloy at room temperature collected from literature sources.[31–40]

MATERIALS AND EXPERIMENTAL METHODS

Ti-6Al-4V powder has been selected as the filler phase to perform material property estimations. The effects of powder particle size distribution, shape, and packing behavior are not considered within the scope of the present work and will be addressed in future studies by our group. The binder used in this work comprised paraffin wax, low-density polyethylene, polypropylene, and stearic acid.

Binder thermomechanical property measurements including density, modulus, specific heat, thermal conductivity, coefficient of thermal expansion, viscosity, and specific volume were conducted at Datapoint Labs (Ithaca, NY) and previously reported by us.[28] These measurements were performed according to the ASTM standards listed in the supplementary Table S-I. Solid density measurements were made for the binder using the Archimedes principle as laid out in ASTM standard D792. A PerkinElmer differential scanning calorimetry (DSC) was used to measure specific heats for the binder following ASTM standard E1269. Thermal conductivity measurements for the binder were made using a K-System II thermal conductivity system following ASTM standard D5930. Viscosity for the binder was measured according to ASTM D3835 using a Goettfert Rheograph capillary rheometer. Pressure-volume-temperature (PVT) measurements for the binder were made with a Gnomix PVT apparatus following ASTM D792. The feedstock properties for the composite with Ti-6Al-4V as filler with polymer binder were estimated using models discussed in the following sections.

For 3D printing experiments, four ASTM E8 tensile samples were printed on an FFF machine (Pulse 3D printer by Matterhackers) with 59 vol.% Ti-6Al-4V powder-polymer feedstock filaments. The preparation of MF^3 filaments was adapted for Ti-6Al-4V based on previous studies that have been reported elsewhere.[12] The print parameters consisted of a layer height of 150 μm, bead width of 550 μm, extrusion temperature of 240 °C, bed temperature of 65 °C, nozzle diameter of 400 μm, and constant print speed of 10 mm/s. For comparison, ABS, a common polymer for FFF printing, was used for 3D printing tensile bar geometries and comparing the attributes of the part with simulations using material properties available in the Digimat-AM material database.

ESTIMATING PROPERTIES OF POWDER-POLYMER MIXTURES

The experimentally measured values of the polymer binder and literature Ti-6Al-4V filler properties were used to estimate feedstock properties of Ti-6Al-4V powder-polymer composite containing 56–60 vol.% solid loading.

Density

The density of a filler-binder mixture is important in MF^3 for calculating thermal stresses, shrinkage, overhang and support structure design, and can be estimated using various available models.[17,18] In this article, an inverse rule of mixtures was used to estimate the composite feedstock density, given in Eq. 1. This model has previously been verified in published work from our group by comparing it with experimental measurements for various fillers.[26,29]

$$\frac{1}{\rho_c} = \frac{X_f}{\rho_f} + \frac{X_b}{\rho_b} \quad (1)$$

where ρ is the density, X is the mass fraction, and the subscripts c, b, and f stand for the composite, binder, and filler, respectively.

Although the feedstock formulation is represented by weight fractions, for preparing powder-polymer mixtures, volumetric comparisons are more useful to compare powders of differing densities. Therefore, the volume fractions of powder and binder were estimated from the mass fractions using Eqs. 2 and 3, respectively:

Table I. Material properties of Ti-6Al-4V alloy at room temperature

Property	Value	Reference
Density (kg/m^3)	4.42 ± 0.06	Refs. 30–37
Specific heat (J/kg K)	560 ± 30	Refs. 35,37–40
Thermal conductivity (W/m K)	6.5 ± 0.4	Refs. 35–40
Coefficient of thermal expansion ($\times 10^{-6}$ K^{-1})	8.8 ± 0.4	Refs. 35–37,39,41,42
Modulus (GPa)	110 ± 3	Refs. 35–39,43,44

$$\phi_f = \frac{\frac{X_f}{\rho_f}}{\frac{X_f}{\rho_f} + \frac{X_b}{\rho_b}} \quad (2)$$

$$\phi_b = 1 - \phi_f \quad (3)$$

where ϕ_f and ϕ_b are the volume fractions of the filler and binder, respectively.

The experimentally obtained solid density for the binder system (ρ_b) (provided in supplementary Table S-II) and the filler properties compiled from the literature (provided in Table I) were used to estimate the solid density of Ti-6Al-4V-binder mixtures as a function of volume fraction using Eq. 1 and shown in Fig. 3a. It was observed that for a change from 0.56 to 0.60 volume fraction of Ti-6Al-4V, the composite solid density increased from 2860 kg/m^3 to 3000 kg/m^3. Further applicability of the model was verified by experimental density measurements for Ti-6Al-4V powder-binder feedstock at 0.59 volume fraction, which was found to be 2950 kg/m^3, representing a deviation $< 0.6\%$ from the estimated value of 2965 kg/m^3. For further verification, estimates of the model to experimental data on a PTFE-TiO_2 system showed a coefficient of determination (R^2) of 0.98, confirming good applicability to make density estimations.[26]

Young's Modulus

The Young's modulus of the feedstock has a direct influence on the strength and distortion of parts fabricated by MF^3. Good adhesion between metal particles and the polymer is essential to achieve a high Young's modulus. Furthermore, solid loading, binder compositions, and temperature strongly influence Young's modulus. Among various models available[19–21] to predict Young's modulus of a filler-polymer mixture, Halpin and Tsai[19] developed a widely accepted model that takes into account the filler shape and loading direction. It has been widely used in studies in predicting the modulus, and its estimates have been verified by experimental data for various filled polymer systems.[45,46] This model is shown in Eq. 4:

$$\frac{E_c}{E_b} = \frac{1 + \xi\eta\phi_f}{1 - \eta\phi_f} \quad (4)$$

where E is the elastic modulus, ξ is a shape parameter dependent on the geometry and loading direction, ϕ is volume fraction, and subscripts c, b, and f stand for the composite, binder, and filler, respectively.

The parameter η is given by Eq. 5:

$$\eta = \frac{E_f/E_b - 1}{E_f/E_b + \xi} \quad (5)$$

The parameter ξ can be approximated to 2 for spherical particles.[19] The Young's modulus for the binder (E_b) was determined experimentally at room temperature (available in supplementary Table S-II) and reported in our prior work.[28] The Ti-6Al-4V filler properties were collected from the literature as shown in Table I. The Young's modulus for intermediate volume fractions was estimated using Eqs. 4 and 5. As seen in Fig. 3b, the modulus changed from 11.4 GPa to 12.8 GPa with the change in volume fraction from 0.56 to 0.60. For verification, estimates of the model to experimental data on an epoxy-glass mixture above 0.4 volume fraction filler showed a coefficient of determination (R^2) of ~ 0.88, confirming good applicability to predict Young's modulus.[26]

Specific Heat

For polymers and metal powder feedstocks, the heat capacity is dependent on the processing temperature. The polymer melting results in phase change and further changes the heat capacity. For MF^3, it is critical to understand the cooling trends that occur in the entire range of processing temperatures. In the current work, a modified rule of mixtures was used[22] as given in Eq. 6 to determine the specific heat of the filler-polymer mixture. This

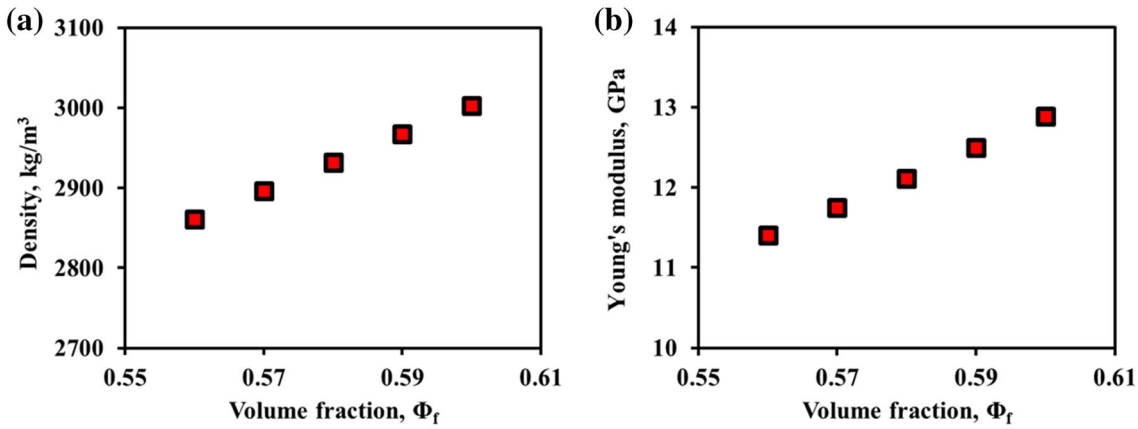

Fig. 3. Estimated (a) density, and (b) Young's modulus for Ti-6Al-4V filler-binder feedstock at different volume fractions.

equation has been successfully applied to mixtures with high volume fraction fillers. In our previous work,[26–29] the predicted values from this model have been evaluated against experimental specific heat measurements and have produced a high coefficient of determination (R^2) of 0.97, suggesting good applicability.

$$C_{p_c} = \left[C_{p_b}X_b + C_{p_f}X_f\right] * \left[1 + A * X_bX_f\right] \quad (6)$$

where A is a correction factor assumed to be 0.2 for spherical particles. C_p is the specific heat, X is the mass fraction, and subscripts c, b, and f stand for the composite, binder, and filler, respectively.

The specific heat for the binder system (C_{p_b}) was experimentally obtained at different temperatures (provided in supplementary Table S-II) as previously reported,[28] and the filler properties were found in the literature (Table I and supplementary Table S-III for each temperature). The values were used to estimate the specific heat capacity over a range of filler volume fractions using Eq. 6 and are plotted in Fig. 4a. Figure 4a shows that for a change from 0.56 to 0.60 volume fraction of Ti-6Al-4V powder at 303 K, the specific heat decreased from 983 J/kg K to 926 J/kg K. With an increase in temperature, the specific heat first increased from 983 J/kg K at 303 K to 1173 J/kg K at 322 K and then decreased to 855 J/kg K at 443 K. Additional data for the specific heat for each volume fraction and temperature are provided in supplementary Table S-III. For verification, estimates of the model to experimental data on a paraffin wax-iron mixture at 0.6 volume fraction filler showed a coefficient of determination (R^2) of 0.99, confirming excellent applicability to predict specific heat.[26]

Thermal Conductivity

The addition of metal particles in the polymer matrix increases the thermal conductivity of MF[3] feedstocks because of the higher thermal conductivity of the metal. In MF[3], the feedstock thermal conductivity is useful in the selection of extruder and built plate temperatures that ensure high density and layer-to-layer bonding. The Bruggeman model shown in Eq. 7 was used to estimate the thermal conductivity of the powder-polymer mixture:

$$1 - \phi_f = \left(\frac{\lambda_f - \lambda_c}{\lambda_f - \lambda_b}\right)\left(\frac{\lambda_b}{\lambda_c}\right)^{1/3} \quad (7)$$

where λ is the thermal conductivity, ϕ is the volume fraction of powder, and the subscripts c, b, and f stand for the composite, binder, and filler, respectively. Equation 7 has been previously reported to predict the thermal conductivity of filled-polymer feedstock systems in reasonable agreement with experimental measurements.[22,26–28,47]

The binder thermal conductivity (λ_b) was experimentally determined (provided in Table S-II) as previously reported,[28] and the filler properties were taken from the literature (Table I); intermediate volume fractions were estimated using Eq. 7 (available in Table S-IV). It can be inferred from Fig. 4b that for a change in volume fraction from 0.56 to 0.60 for Ti-6Al-4V powder at 316 K, the thermal conductivity increased from 1.3 W/m K to 1.5 W/m K. With an increase in temperature from 316 K to 438 K at 0.59 volume fraction, the thermal conductivity first increased from 1.47 W/m K to 1.50 W/m K at 357 K and then decreased to 1.41 W/m K at 438 K. The trend was similar for other volume fractions of Ti-6Al-4V feedstocks. The trend of the curve for the composite feedstock is

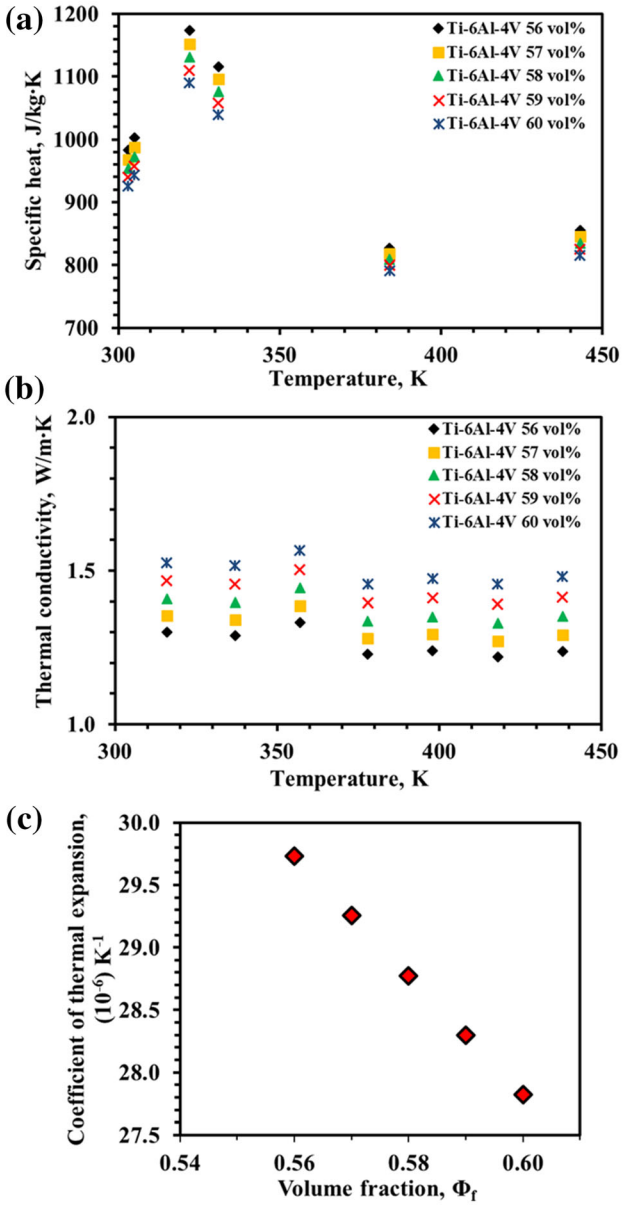

Fig. 4. Estimated thermal properties of composite Ti-6Al-4V powder-binder feedstock at different volume fractions for (a) specific heat as a function of temperature, (b) thermal conductivity as a function of temperature, and (c) coefficient of thermal expansion.

dominated by the thermal conductivity of the matrix/binder material. The typical crest and trough observed in the curve are due to the changes in the binder state from solid to liquid while being heated to a definitive temperature. For verification, estimates of the model to experimental data on PLA-aluminum mixture above 0.5 volume fraction filler showed a coefficient of determination (R^2) of $\sim$ 0.9, confirming good applicability to predict thermal conductivity.[26]

Coefficient of Thermal Expansion (CTE)

Three-dimensional printed components expand and shrink during the heating and cooling stages of the process. Uneven temperature distributions can cause warping in parts due to the buildup of residual thermal stresses while cooling. Thermal stresses are proportional to the CTE of powder-polymer mixtures, which can be calculated by several models.[24–28] The general rule of mixtures shown in Eq. 8 requires fewer empirical constants compared with other models.

$$\alpha_c = \phi_f \alpha_f + \alpha_b(1 - \phi_f) \tag{8}$$

where α is the thermal expansion coefficient, ϕ is the volume fraction, and the subscripts c, f, and b stand for the composite, filler, and binder, respectively. In our previous work,[26] when evaluated against experimental values it yields a regression coefficient of determination (R^2) in the range of 0.87–0.97, indicating a good fit.

The CTE for binder (α_b) was experimentally obtained (see Table S-II), and the filler properties were found in the literature, provided in Table I, while the values for intermediate volume fractions were estimated using Eq. 8. In Fig. 4c, for a change in volume fraction from 0.56 to 0.60, the CTE decreased from 29.7×10^{-6} K^{-1} to 27.8×10^{-6} K^{-1}. For verification, estimates of the model to experimental data on an epoxy-alumina mixture at 0.5 volume fraction filler showed a coefficient of determination (R^2) of $\sim$ 0.9, confirming good applicability to predict CTE.[26]

Viscosity

In MF^3, the molten feedstock material flows through the nozzle to form the desired geometry. The rheological understanding of powder-polymer mixtures is crucial since at higher powder loadings the feedstock viscosity increases. The typical filler content ranges between 50 vol.% and 65 vol.%, and the viscosity varies as the inverse of powder particle size. Rheological characteristics provide clear understanding related to flow instabilities while printing and thereby the influence of powder loading, shear rate, and temperature on the material flow properties.

The Krieger-Dougherty model[26–28,48] has been found suitable for predicting viscosity values for highly filled powder-polymer mixtures from our previous work, generating a coefficient of determination (R^2) ranging from 0.94 to 0.99 compared with experimental viscosity measurements. A simplified form of the model is given in Eq. 9:

$$\eta_c = \frac{\eta_b}{\left[1 - \frac{\phi_f}{\phi_m}\right]^2} \tag{9}$$

where η is the viscosity. Subscripts c and b stand for the composite and binder, respectively. ϕ_m stands for the maximum packing fraction of the filler and is approximated to be 0.64 for randomly packed spheres,[49] and ϕ_f is the filler volume fraction.

Figure 5 shows the variation in viscosity as a function of powder volume fraction, shear rate, and temperature (tabulated data provided in supplementary Table S-V). At 413 K and a shear rate of 800 s^{-1}, increasing the volume fraction of powder from 0.56 to 0.60 increases the viscosity from 840 Pa s to 3350 Pa s. For example, for a volume fraction of 0.59 at 423 K with an increasing shear rate from 20 s^{-1} to 1600 s^{-1}, the viscosity decreases one order of magnitude from 5130 Pa s to 590 Pa s. Similarly, increasing the temperature from 413 K to 423 K decreases the viscosity from 2140 Pa s to 840 Pa s for 0.59 volume fraction at 800 s^{-1}. For processes operating under low shear rates, it is highly important to have low feedstock viscosity for successful flowability, especially for the MF^3 process where the filament strength properties provide enough force for a continuous flow through the nozzle and successful printing operation. Experimental viscosity measurements for 0.59 volume fraction Ti-6Al-4V powder-binder feedstock at 423 K and 160 s^{-1} was found to be 600 Pa s, representing an overestimated value of 2070 Pa s. The differences in the particle packing behavior of Ti-6Al-4V powder may result in $\phi_m > 0.64$ for the viscosity prediction of randomly packed, monosized spheres, resulting in overestimation compared with experimental data. For additional verification, estimates of the model to experimental data on an LDPE-alumina mixture at 0.6 volume fraction filler showed a coefficient of determination (R^2) of $\sim$ 0.95, confirming good applicability to predict viscosity for the system.[26]

Viscosity is sensitive to shear rate and temperature. At low temperatures, the mixture viscosity is high, making it difficult to print. At high temperatures, the binder could break down or powder-binder separation could result during extrusion. Therefore, a bounded range of conditions is likely to exist across which successful printing is best achieved. The Cross-WLF equation can be used to numerically capture the shear rate and temperature changes in viscosity,[50] as shown in Eq. 10:

$$\eta = \frac{\eta_0}{1 + \left(\frac{\eta_0 \dot{\gamma}}{\tau^*}\right)^{1-n}} \tag{10}$$

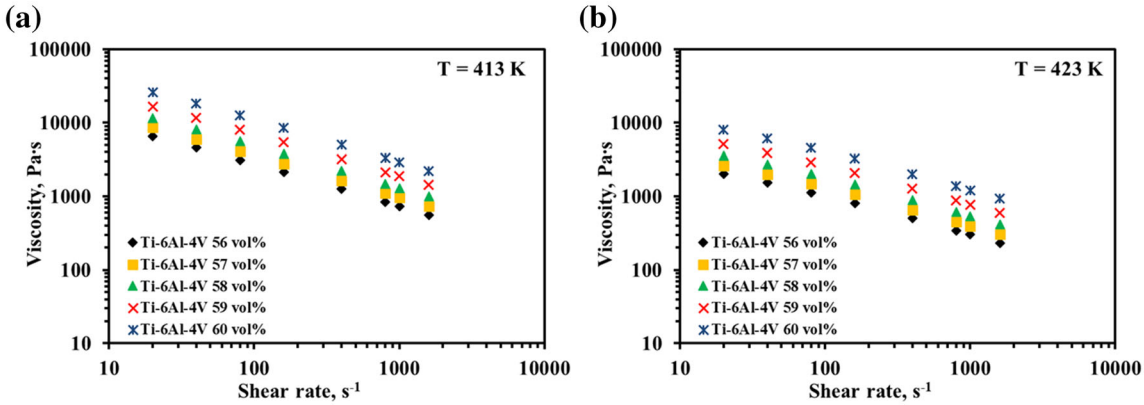

Fig. 5. Estimated viscosity of the Ti-6Al-4V powder-binder feedstock for a shear rate of 20–1600 s^{-1} at (a) 413 K, and (b) 423 K with different volume fractions.

where η is the melt viscosity (Pa s), η_0 is the zero shear viscosity (Pa s), $\dot{\gamma}$ is the shear rate (s^{-1}), τ^* is the critical stress level at the transition to shear thinning (Pa), which is determined by curve fitting, and n is the power-law index in the high shear rate regime, also determined by curve fitting.

The viscosity of a filled polymer mixture and its temperature dependence can be calculated using Eq. 11:

$$\eta_0 = D_1 \exp\left[-\frac{A_1(T-T^*)}{A_2+(T-T^*)}\right] \tag{11}$$

where T is the temperature (K), T^*, D_1, and A_1 are curve fitted coefficients, and A_2 (assumed as 51.6) is the WLF constant. The values of these coefficients can be obtained by curve fitting the estimated viscosity for different volume fractions of powder at various shear rates and temperatures. Representative extracted cross WLF constants for a 59 vol.% solid loading Ti-6Al-4V feedstock are provided in supplementary Table S-VI.

Specific Volume

Warpage and non-uniform shrinkage during cooling are some of the reported issues in the polymer FFF process That are equally important in MF^3. The variation in specific volume as a function of temperature and pressure could help provide substantial information in mitigating dimensional variations during shrinkage of MF^3 parts. The specific volume also depends on the filler volume fraction and was calculated using the rule of mixtures[17] shown in Eq. 12. The rule of mixtures has been found to be a reliable method in predicting the specific volume of polymer filled systems, with our previous work[26] producing a high coefficient of determination (R^2) of 0.99 compared with experimental results.

$$\upsilon_c = X_f\upsilon_f + \upsilon_b(1-X_f) \tag{12}$$

where υ is the specific volume, X is the mass fraction, and the subscripts c, f, and b refer to the composite, filler, and binder, respectively.

Figure 6 shows the variation of specific volume on the temperature, pressure, and powder volume fraction (data available in Table S-VII). Increasing the volume fraction from 0.56 MPa to 0.60 at 0 MPa decreased the specific volume from 3.51×10^{-4} m^3/kg to 3.34×10^{-4} m^3/kg at 300 K. When the temperature was increased from 300 K to 450 K at 0 MPa, the specific volume increased from 3.51×10^{-4} m^3/kg to 3.87×10^{-4} m^3/kg for feedstock with a 0.56 volume fraction of Ti-6Al-4V powder. However, with increasing pressure from 0 MPa to 50 MPa (at 300 K and 0.56 volume fraction), the specific volume was found to decrease from 3.51×10^{-4} m^3/kg to 3.48×10^{-4} m^3/kg. For additional verification, estimates of the model to experimental data on a PP-aluminum mixture at 0.5 volume fraction filler showed a coefficient of determination (R^2) of 0.99, confirming good applicability to predict the specific volume for the system.[26]

A two-domain Tait[50] model (Eq. 13) can be used for generating specific volume data as a function of temperature and pressure pertaining to the MF^3 processing conditions:

$$\upsilon(T,p) = \upsilon_0(T)\left[1 - C\ln\left(1+\frac{p}{B(T)}\right) + \upsilon_t(T,p)\right] \tag{13}$$

where $\upsilon(T,p)$ is the specific volume at a given temperature and pressure, $\upsilon_0(T)$ is the specific volume at zero gauge pressure, T is the temperature in K, p is pressure in Pa, and C is a constant assumed to be 0.0894 for the two-domain Tait model. The parameter $B(T)$, accounts for the pressure sensitivity of the material and is separately defined for the solid and melt regions. For the upper bound[50] when $T > T_t$ (volumetric transition temperature), the parameters, υ_0, B and $\upsilon(T,p)$ are given by Eqs. 14, 15 and 16 respectively.

$$\upsilon_0 = b_{1m} + b_{2m}(T - b_5) \tag{14}$$

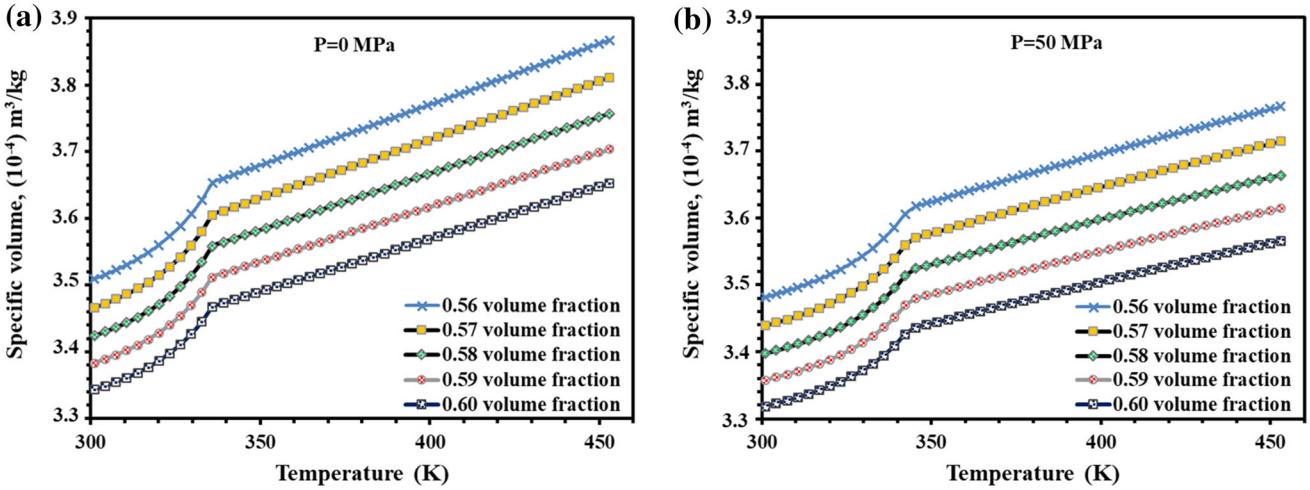

Fig. 6. Estimated specific volume of Ti-6Al-4V powder-binder feedstock at different filler volume fractions for (a) 0 MPa, and (b) 50 MPa.

$$B(T) = b_{3m}e^{[-b_{4m}(T-b_5)]} \quad (15)$$

$$\upsilon_t(T,p) = 0 \quad (16)$$

where b_{1m}, b_{2m}, b_{3m}, b_{4m}, and b_5 are curve-fitted coefficients. For the lower bound,[50] when $T < T_t$, the parameters, υ_0, B and $\upsilon(T,p)$ are given by Eqs. 17, 18 and 19 respectively.

$$\upsilon_0 = b_{1s} + b_{2s}(T - b_5) \quad (17)$$

$$B(T) = b_{3s}e^{[-b_{4s}(T-b_5)]} \quad (18)$$

$$\upsilon_t(T,p) = b_7e^{[b_8(T-b_5)-(b_9p)]} \quad (19)$$

where b_{1s}, b_{2s}, b_{3s}, b_{4s}, b_5, b_7, b_8, and b_9 are the curve-fitted coefficients. The dependence of the volumetric transition temperature, T_t, on pressure can be given by Eq. 20:

$$T_t(p) = b_5 + b_6(p) \quad (20)$$

Representative extracted dual-domain Tait constants for 59 vol.% solid loading Ti-6Al-4V feedstock are provided in supplementary Table S-VIII.

SIMULATION CASE STUDY RESULTS

In the current study, Digimat-AM® was used as a simulation tool that takes material thermophysical properties as the input parameters. Here, material properties for the 59 vol.% Ti-6Al-4V powder-polymer feedstock system estimated using the models presented previously were used as input parameters to predict warpage/dimensional changes for a tensile bar printed with MF^3.

Figure 7a shows the CAD file with dimensions for an ASTM E8 tensile sample. The part dimensions of this geometry obtained from simulations and MF^3 experiments were in excellent agreement (data provided in supplementary Fig. S-1). Warpage analyses of simulated and fabricated samples of 59 vol.% Ti-6Al-4V MF^3 samples are shown in Fig. 7b and c, respectively. Simulation results predicted the maximum warpage was located at the edge of the tensile bar and the magnitude of warpage at this location along the Z direction was 0.07 mm. In close agreement with simulations, the MF^3 experiments with the green parts verified that the location of the maximum warpage was identical. However, the magnitude of the warpage at this location in the Z direction was slightly higher at 0.3 ± 0.04 mm. To further assess the differences between MF^3 and FFF results, simulations and experiments were also conducted on a standard ABS polymer for the same tensile bar specimen and are represented in Fig. 7d and e. For ABS parts from simulations, the location of maximum warpage was identical to the MF^3 simulation result. However, the magnitude of warpage at this location in the Z direction was comparatively higher at 0.14 mm. In FFF experiments with ABS, the location of maximum warpage correlated with the ABS simulation. However, the magnitude measured in the Z direction was also slightly higher at 0.7 ± 0.15 mm. The warpage results obtained from simulations as well as experiments are summarized in Fig. 7f. These results indicate that the location of maximum warpage is accurately predicted for both material systems. However, the magnitude of warpage is under-estimated by the Digimat-AM® simulation platform for both systems and needs further analysis and refinement in the future. Typically, uneven heat distribution creates internal stresses within a part, resulting in warpage.[51,52] Several material properties are known to contribute to the overall warpage. However, the CTE value of the 59 vol.% Ti-6Al-4V powder-binder system (2.8×10^{-5} K^{-1}) is lower than that for ABS (9×10^{-5} K^{-1}) and is concluded to be the major reason for the differences in the extent of warpage in the two material systems.

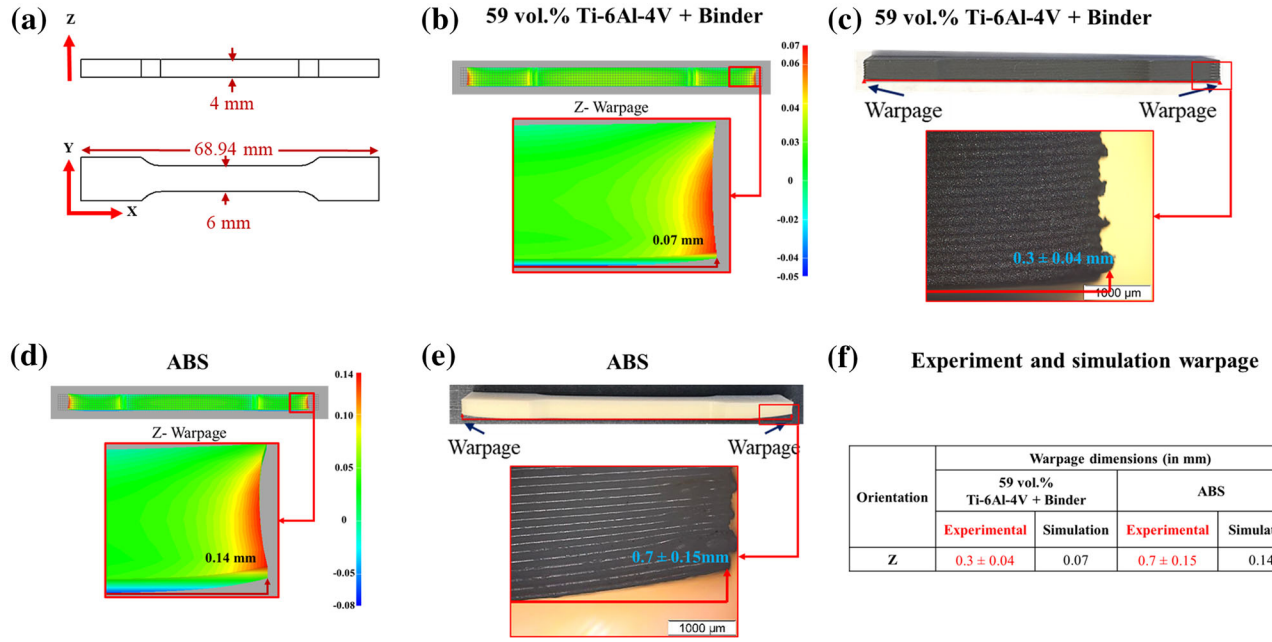

Orientation	Warpage dimensions (in mm)			
	59 vol.% Ti-6Al-4V + Binder		ABS	
	Experimental	Simulation	Experimental	Simulation
Z	0.3 ± 0.04	0.07	0.7 ± 0.15	0.14

Fig. 7. Experimental and simulation result verifications using estimated values: (a) CAD file for ASTM E8 tensile sample with dimensions. (b) Simulation of the part using the estimated material properties for 59 vol.% Ti-6Al-4V + binder feedstock. (c) Printed green parts with 0.59 vol.% of Ti-6Al-4V + binder feedstock. (d) Simulation of the ABS part using the available material database in Digimat-AM®. (e) Printed part with ABS material filament. (f) Warpage analysis resulting from experiments and simulation for 59 vol.% Ti-6Al-4V + binder feedstock and ABS (Color figure online).

The above results suggest the potential for using the material property estimation protocol for analyzing complex geometries using other output parameters of the MF^3 process including warpage, residual stresses, porosity, and distortion. Preliminary results demonstrating the geometry capability are shown in supplementary Fig. S-2. These studies are currently underway in our group and will be reported in the future. Supplementary Table S-IX provides material properties for the other most commonly used metals that can be used to estimate input material properties for other MF^3 systems based on the protocols presented in the present study. These studies are also currently underway in our group and will be reported in future publications.

CONCLUSION

Based on the estimated metal-polymer mixture properties and their use in process simulations, the following conclusions can be drawn:

- The variation of material properties related to dimensional changes as a function of filler attributes and filler volume fraction can be estimated for Ti-6Al-4V powder-polymer mixtures.
- The properties estimated using various models enable the evaluation of component-level attributes fabricated by MF^3 using DfMF^3 platforms. The component-level attributes included here are the final dimensions and warpage.
- The overall approach enables the understanding of the dependence of MF^3 processing of complex Ti-6Al-4V components on the material composition.
- The experimental protocols for verifying the estimated material properties presented in this work can help in further refining the models and analyzing their influence on successfully predicting MF^3 outcomes.
- It is expected that the overall approach will help reduce significant trial and error in designing new materials that can be used to fabricate complex geometries using MF^3.

ACKNOWLEDGEMENT

The authors acknowledge financial assistance from the Minority Business Development Agency of the US Department of Commerce as well as NASA through a subcontract from Techshot. The authors also acknowledge MSC Software, AlphaSTAR, and Vanderplaats R&D for their support in providing AM software platforms.

ELECTRONIC SUPPLEMENTARY MATERIAL

The online version of this article (https://doi.org/10.1007/s11837-019-03920-y) contains supplementary material, which is available to authorized users.

REFERENCES

1. J. Gonzalez-Gutierrez, S. Cano, S. Schuschnigg, C. Kukla, J. Sapkota, and C. Holzer, *Materials* 11, 840 (2018).
2. R.M. German, *Injection molding of metals and ceramics*, 1st ed. (Princeton: Metal Powder Industries Federation, 1997), pp. 83–98.
3. S. Rangarajan, G. Qi, N. Venkataraman, A. Safari, and S.C. Danforth, *J. Am. Ceram. Soc.* 83, 1663 (2000).
4. G. Wu, N.A. Langrana, R. Sadanji, and S. Danforth, *Mater. Des.* 23, 97 (2002).
5. W. Lengauer, I. Duretek, M. Fürst, V. Schwarz, J. Gonzalez-Gutierrez, S. Schuschnigg, C. Kukla, M. Kitzmantel, E. Neubauer, and C. Lieberwirth, *Int. J. Refract. Met. Hard Mater.* 82, 141 (2019).
6. S. Masood and W. Song, *Mater. Des.* 25, 587 (2004).
7. M. Nikzad, S. Masood, and I. Sbarski, *Mater. Des.* 32, 3448 (2011).
8. D.A. Anderegg, H.A. Bryant, D.C. Ruffin, S.M. Skrip Jr, J.J. Fallon, E.L. Gilmer, and M.J. Bortner, *Addit. Manuf.* 26, 76 (2019).
9. M.K. Agarwala, V.R. Jamalabad, N.A. Langrana, A. Safari, P.J. Whalen, and S.C. Danforth, *Rapid Prototyp. J.* 2, 4 (1996).
10. A. Bose, C.A. Schuh, J.C. Tobia, N. Tuncer, N.M. Mykulowycz, A. Preston, A.C. Barbati, B. Kernan, M.A. Gibson, and D. Krause, *Int. J. Refract. Met. Hard Mater.* 73, 22 (2018).
11. J. Gonzalez-Gutierrez, F. Arbeiter, T. Schlauf, C. Kukla, and C. Holzer, *Mater. Lett.* 248, 165 (2019).
12. B. Barmore, Fused Filament Fabrication of Filled Polymers for Metal Additive Manufacturing. Master's Thesis (Mechanical Engineering, Oregon State University, 2016), pp. 55–60.
13. L. Ren, X. Zhou, Z. Song, C. Zhao, Q. Liu, J. Xue, and X. Li, *Materials* 10, 305 (2017).
14. e-xstream, Digimat-AM simulation solution for Additive Manufacturing. https://www.e-xstream.com/product/digimat-am. Accessed 30 July 2019.
15. Alphastar, Genoa Additive Manufacturing design tool and software suite for polymers, metals and ceramics. http://www.alphastarcorp.com/products/genoa-3dp-simulation/. Accessed 30 July 2019.
16. Vanderplaats, Genesis structural analysis and optimization software. http://www.vrand.com/products/genesis/. Accessed 30 July 2019.
17. L.E. Nielsen, *Predicting the Properties of Mixtures*, 1st ed. (New York: M. Dekker, 1978), pp. 5–11.
18. S. McGee and R. McGullough, *Polym. Compos.* 2, 149 (1981).
19. W. Wu, K. Sadeghipour, K. Boberick, and G. Baran, *Mater. Sci. Eng. A* 332, 362 (2002).
20. T.J. Wooster, S. Abrol, J.M. Hey, and D.R. MacFarlane, *Compos. Part A* 35, 75 (2004).
21. I. Balać, M. Milovančević, C.-Y. Tang, P.S. Uskoković, and D.P. Uskoković, *Mater. Lett.* 58, 2437 (2004).
22. Y.P. Mamunya, V. Davydenko, P. Pissis, and E. Lebedev, *Eur. Polym. J.* 38, 1887 (2002).
23. L. Kowalski, J. Duszczyk, and L. Katgerman, *J. Mater. Sci.* 34, 1 (1999).
24. A. Boudenne, L. Ibos, M. Fois, E. Gehin, and J.C. Majeste, *J. Polym. Sci. Part B Polym. Phys.* 42, 722 (2004).
25. T. Zhang, J. Evans, and K. Dutta, *J. Eur. Ceram. Soc.* 5, 303 (1989).
26. K.H. Kate, R.K. Enneti, S.-J. Park, R.M. German, and S.V. Atre, *Crit. Rev. Solid State Mater. Sci.* 39, 197 (2014).
27. K.H. Kate, R.K. Enneti, V.P. Onbattuvelli, and S.V. Atre, *Ceram. Int.* 39, 6887 (2013).
28. K.H. Kate, V.P. Onbattuvelli, R.K. Enneti, S.W. Lee, S.J. Park, and S.V. Atre, *JOM* 64, 1048 (2012).
29. K.H. Kate, R.K. Enneti, T. McCabe, and S.V. Atre, *Ceram. Int.* 42, 194 (2016).
30. N.M. Nor, N. Muhamad, M. Ibrahim, M. Ruzi, and K. Jamaludin, *Int. J. Mech. Mater. Eng.* 6, 126 (2011).
31. G. Shibo, Q. Xuanhui, H. Xinbo, Z. Ting, and D. Bohua, *J. Mater. Process. Technol.* 173, 310 (2006).
32. G. Obasi, O. Ferri, T. Ebel, and R. Bormann, *Mater. Sci. Eng. A* 527, 3929 (2010).
33. E. Ergül, H. Özkan Gülsoy, and V. Günay, *Powder Metall.* 52, 65 (2009).
34. H.Ö. Gülsoy, N. Gülsoy, and R. Calışıcı, *Bio-Med. Mater. Eng.* 24, 1861 (2014).
35. K.C. Mills, *Recommended Values of Thermophysical Properties for Selected Commercial Alloys* (Cambridge: Woodhead Publishing, 2002), pp. 211–215.
36. G. Welsch, R. Boyer, and E. Collings, *Materials Properties Handbook: Titanium Alloys* (Ohio: ASM International, 1993), pp. 514–520.
37. R. Enneti, V. Onbattuvelli, O. Gulsoy, K. Kate, and S. Atre, *Powder-Binder Formulation and Compound Manufacture in Metal Injection Molding (MIM). Handbook of Metal Injection Molding*, 2nd ed. (Cambridge: Woodhead Publishing, 2002), pp. 57–88.
38. G. Chen, C. Ren, X. Yang, X. Jin, and T. Guo, *Int. J. Adv. Manuf. Technol.* 56, 1027 (2011).
39. C.J. Smithells, *Metals Reference Book*, 5th ed. (Oxford: Butterworth Publishing, 1976), pp. 1148–1152.
40. V. Wagner, M. Baili, G. Dessein, and D. Lallement, *Key Eng. Mater.* 446, 147 (2010).
41. J. Elmer, T. Palmer, S. Babu, and E. Specht, *Mater. Sci. Eng. A* 391, 104 (2005).
42. R. Rai, J. Elmer, T. Palmer, and T. DebRoy, *J. Phys. D Appl. Phys.* 40, 5753 (2007).
43. M. Niinomi, *Mater. Sci. Eng. A* 243, 231 (1998).
44. Y. Lee and G. Welsch, *Mater. Sci. Eng. A* 128, 77 (1990).
45. Y.P. Wu, Q.-X. Jia, D.-S. Yu, and L.-Q. Zhang, *Polym. Test.* 23, 903 (2004).
46. C.L. Tucker and E. Liang, *Compos. Sci. Technol.* 59, 655 (1999).
47. C. Wong and R.S. Bollampally, *J. Appl. Polym. Sci.* 74, 3396 (1999).
48. A. Metzner, *J. Rheol.* 29, 739 (1985).
49. R.M. German, *J. Am. Ceram. Soc.* 77, 283 (1994).
50. H. Chiang, C. Hieber, and K. Wang, *Polym. Eng. Sci.* 31, 116 (1991).
51. A.H. Peng, *Adv. Mater. Res.* 538–541, 1564 (2012).
52. B.N. Turner and S.A. Gold, *Rapid Prototyp. J.* 21, 250 (2015).